Science of the Total Environment 566–567 (2016) 230–237

Contents lists available at ScienceDirect

Science of the Total Environment

journal homepage: www.elsevier.com/locate/scitotenv

Identification of chemical compositions and sources of atmospheric aerosols in Xi'an, inland China during two types of haze events

Jianjun Li [a,b], Gehui Wang [a,b,c,d,*], Yanqin Ren [a,e], Jiayuan Wang [a,e], Can Wu [a,e], Yanni Han [a,e], Lu Zhang [a,e], Chunlei Cheng [a,e], Jingjing Meng [a,e]

[a] Key Laboratory of Aerosol Chemistry and Physics, Institute of Earth Environment, Chinese Academy of Sciences, Xi'an 710061, China
[b] State Key Laboratory of Loess and Quaternary Geology, Institute of Earth Environment, Chinese Academy of Sciences, Xi'an 710061, China
[c] School of Human Settlements and Civil Engineering, Xi'an Jiaotong University, Xi'an 710079, China
[d] Center for Excellence in Urban Atmospheric Environment, Institute of Urban Environment, Chinese Academy of Sciences, Xiamen 361021, China
[e] University of Chinese Academy of Sciences, Beijing 100049, China

HIGHLIGHTS

- Hourly changes in chemical compositions of aerosols were quantified.
- Aerosols in the Light-haze event are characteristic of dust-related species.
- Aerosols in the Severe-haze are characteristic of secondary inorganic species.
- Sulfate and nitrate production is more efficient than SOA in haze periods.

GRAPHICAL ABSTRACT

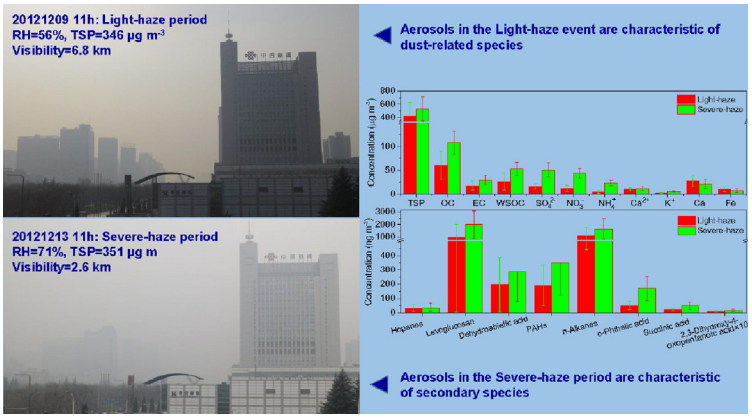

ARTICLE INFO

Article history:
Received 1 March 2016
Received in revised form 7 May 2016
Accepted 9 May 2016
Available online xxxx

Editor: D. Barcelo

Keywords:
TSP and haze
Relative humidity
Sulfate, nitrate and dust
Primary and secondary organic aerosols

ABSTRACT

High time resolution (1 h) of TSP filter samples was collected in Xi'an in inland China from December 5 to 13, 2012, during which a 9-day long of haze episode occurred. The hazy days were classified as two types, i.e., Light-haze period with moderate degradation in visibility (5–10 km) and relatively dry conditions (RH: 53 ± 19%) and Severe-haze period with a daily visibility less than 5 km and humid conditions (RH: 73 ± 14%). TSP in the two periods (415 ± 205 and 530 ± 180 μg m^{-3} in Light-haze and Severe-haze periods, respectively) was comparable, but crustal Fe and Ca elements presented higher concentrations and strong correlation (R^2 = 0.72) with TSP in Light-haze period. SO_4^{2-}, NO_3^- and NH_4^+ in Light-haze period were 16 ± 5.9, 12 ± 6.7 and 4.1 ± 2.8 μg m^{-3}, respectively, and increased dramatically to 51 ± 15, 44 ± 9.7 and 23 ± 5.6 μg m^{-3} in Severe-haze period. Contributions of Fe and Ca to TSP decreased from 9.2% in Light-haze period to 5.3% in Severe-haze period, but those of SO_4^{2-}, NO_3^- and NH_4^+ increased from 3.8%, 2.9% and 1.0% in Light-haze period to 9.6%, 8.3% and 4.4% in Severe-haze period, respectively. These results suggest that dust-derived particles were more significant in Light-haze period while secondary aerosols were more important in Severe-haze period. Hopanes (33 ± 24 and 38 ± 29 ng m^{-3} in Light-haze and Severe-haze periods, respectively) during the two types of haze

* Corresponding author at: Key Laboratory of Aerosol Chemistry and Physics, Institute of Earth Environment, Chinese Academy of Sciences, Xi'an 710061, China.
E-mail addresses: wanggh@ieecas.cn, gehuiwang@yahoo.com.cn (G. Wang).

http://dx.doi.org/10.1016/j.scitotenv.2016.05.057

periods are comparable, indicating that differences in contribution of primary organic aerosols from fossil fuel combustions to TSP were insignificant. In contrast, the ratio of secondary organic aerosols (e.g., *o*-phthalic acid) to EC was much higher in Severe-haze period (5.8 ± 2.7 ng μg^{-1}) than in Light-haze period (3.4 ± 2.1 ng μg^{-1}), probably indicating that the humid conditions in Severe-haze period are favorable for secondary organic aerosol formation.

1. Introduction

Air pollution in China has been a persistent problem because of tremendous air pollutants such as SO_2, NOx, elemental carbon (also called as black carbon) and volatile organic compounds (VOCs) emitted from power plants, industry and vehicles due to rapid economy development. The emitted pollutants affect not only the local air quality but also the global climate via a long-range transport. Therefore, air pollution in China has been a major concern worldwide (Guo et al., 2014; Huang et al., 2014; Menon et al., 2002; Streets and Waldhoff, 2000). In order to efficiently reduce the pollutant emissions, numerous studies have been conducted to investigate the sources and formation mechanisms of haze in the country. However, these studies mostly focused on its east coastal developed regions such as Beijing–Tianjin region (Quan et al., 2011; Zhao et al., 2013), Yangtze River Delta (Q. Fu et al., 2008; Wang et al., 2014a; Ye et al., 2011) and Pearl River Delta (Tan et al., 2009), and information of air pollution in inland China is limited. Due to differences in energy compositions, economy development levels and climate conditions air pollution characteristics in inland China are significantly different from that in east coastal China. For instance, in the past five years SO_2 levels in Beijing and Shanghai have sharply decreased, resulting in nitrate in fine particles exceeding over sulfate (Y.L. Sun et al., 2013; Zhao et al., 2015). In contrast, sulfate is still the dominant species of fine particles in inland China because of the predominance in coal combustion for energy consumption (Li et al., 2014). Moreover, owing to limited precipitation airborne particles from some regions of inland China are often enriched in dust (Zhang et al., 2015). Therefore, China is a large and diverse source of aerosols and trace gases to the atmosphere.

Xi'an (34.27° N, 108.90° E) is located in Guanzhong Basin, a semiarid region in inland China, and is one of the most heavily polluted megacities in the country with an annual concentration of $PM_{2.5}$ on the ground surface more than 80 μg m^{-3} during 2001–2006 (van Donkelaar et al., 2010). Xi'an has consumed a huge amount of energy in recent years due to economy expansion. For example, the annual total energy consumption of Xi'an in 2012 reached 9.9×10^6 tons of SCE (standard coal equivalent), while the annual vehicle number of the city in 2012 was about 1.6×10^6 (Xi'an Municipal Bureau of Statistics and NBS Survey Office in Xi'an, 2013). Considering the basin-like topography and semiarid climate, such a high level of $PM_{2.5}$ suggests that the chemical composition and sources of atmospheric aerosols in Guanzhong Basin including Xi'an are probably different from those in the east coastal regions. For example, Huang et al. (2014) compared the chemical compositions and sources of $PM_{2.5}$ in Beijing, Shanghai, Guangzhou and Xi'an during the heavy hazy period of January 2013 and found that aerosols in Xi'an were more affected by dust. In the current work TSP filter samples were collected with a 1-hour time resolution at the urban center of Xi'an from December 5th to 13th, 2012, and analyzed for organic carbon (OC), elemental carbon (EC), inorganic ions, elements and organic molecules in order to understand the origin and formation mechanism of haze problem in the city. Our results revealed two types of hazes in Xi'an, which are characterized by primary emissions from dust with a low relative humidity and secondary components with a high relative humidity, respectively.

2. Experimental section

2.1. Sample collection

TSP samples were collected on the rooftop (10 m above the ground) of a three-story building on the campus of the Institute of Earth Environment, Chinese Academy of Sciences, which is located in the urban center of Xi'an (Fig. S1). The sampling was conducted from December 5 to 13, 2012 by alternately using two high volume (1.0 m^3 min^{-1}) samplers (same mode produced by Wuhan Tianhong Instruments Co., Ltd, China) with 1 h duration in each. The two samplers were calibrated before the sampling. A total of 202 hourly samples were collected onto pre-baked (450 °C, 6–8 h) quartz fiber filters. Field blank samples were also collected by mounting blank filters onto the sampler for about 10 min without pumping any air. After sampling, the filter samples were individually sealed in aluminum foil bags and stored in a freezer (−20 °C) prior to analysis.

2.2. Sample analysis

2.2.1. Organic compounds

A 12.5 or 25 cm^{-2} punch of the sample/blank filter was cut and extracted with a mixture of dichloromethane and methanol (2:1, v/v) under ultrasonication. The extracts were concentrated using a rotary evaporator under vacuum conditions and then blow down to dryness using pure nitrogen. After reaction with N,O-bis-(trimethylsilyl) trifluoroacetamide (BSTFA) at 70 °C for 3 h, the derivatives were determined using gas chromatography/mass spectrometry (GC/MS).

GC/MS analysis of the derivatives was performed using an Agilent 7890A GC coupled with an Agilent 5975C MSD. The GC separation was carried out using a DB-5MS fused silica capillary column with the GC oven temperature programmed from 50 °C (2 min) to 120 °C at 15 °C min^{-1} and then to 300 °C at 5 °C min^{-1} with a final isothermal hold at 300 °C for 16 min. The sample was injected in a splitless mode at an injector temperature of 280 °C, and scanned from 50 to 650 Da using electron impact (EI) mode at 70 eV. GC–MS response factors (RF) of most target compounds were determined using the authentic standards. RF of 2,3-dihydroxy-4-oxopentanoic acid were replaced by that of succinic acid because the standard is not commercially available. Limits of detection (LOD) and quantitation (LOQ) of the target compounds were calculated based on a signal-to-noise ratio (SNR) approach. Signal-to-noise ratios of 3:1 and 10:1 were considered for the estimations of LOD and LOQ in the current study. LOD and LOQ were in the range of 0.004–0.122 and 0.012– 0.407 μg L^{-1}, respectively, for all organic compounds studied. The accuracy of the methodology is 98.2%, determined by the error obtained between the mean value of triplicates of a standard solution of 2 μg L^{-1}. The precision of the methodology is 5.6%, calculated as the relative standard deviation (%RSD). No significant contamination (<5% of those in the samples) was found in the blanks. Recoveries of all the target compounds ranged from 80% to 120%. Data presented were corrected for the field blanks but not corrected for the recoveries.

2.2.2. EC, OC, inorganic ions, WSOC, WSIC and elements

OC (organic carbon) and EC (elemental carbon) were analyzed using DRI Model 2001 Carbon Analyzer following the Interagency Monitoring of Protected Visual Environments (IMPROVE) thermal/optical reflectance (TOR) protocol. Sample filter was placed in a quartz boat inside the analyzer and gradually heated to temperatures of 140 °C (OC1), 280 °C (OC2), 480 °C (OC3), and 580 °C (OC4) in a non-oxidizing helium (He) atmosphere, and 580 °C (EC1), 740 °C (EC2), and 840 °C (EC3) in an oxidizing atmosphere of 2% oxygen in helium. Pyrolyzed carbon (PC) is determined by reflectance and transmittance of 633 nm light. The analyzer was calibrated with a known quantity of CH_4 every day. One sample was randomly selected from 10 samples and re-analyzed. Differences determined from the replicate analyses were < 5% for TC and < 10% for OC and EC.

A portion of the filter was cut and extracted with 40 mL Milli-Q water under sonication (15 min each, repeated 3 times) and filtered through a PTFE filter to remove any particles and filter debris. Then the water-extract was divided into two parts. One part was used for inorganic ion analysis using ion chromatography (Dionex 600, Dionex, US). The detection limits were lower than 0.05 mg L^{-1} for both anions and cations. The second part of the water-extract was analyzed for water-soluble organic (WSOC) and inorganic carbon (WSIC) using a TOC analyzer (TOC-L CPH, Shimadzu, Japan).

Elemental compositions were determined by energy dispersive X-ray fluorescence (ED-XRF) spectrometry (Epsilon 5 ED-XRF, PANalytical B.V., Netherlands). Each sample was analyzed for 30 min to obtain a spectrum of X-ray counts versus photon energy with the individual peak energies matching specific elements and peak areas corresponding to elemental concentrations. The spectrometer was calibrated with thin-film standards obtained from MicroMatter Co. (Arlington, WA, USA).

All carbonaceous components, inorganic ions and element data reported here were corrected by the field blanks (less than 10% of those in the ambient samples).

3. Results and discussion

3.1. Meteorological condition and TSP concentration

Based on the meteorological condition and TSP concentration variation (Fig. 1), the sampling campaign can be classified as three periods. (1) Clean period, from the sampling beginning hour to December 5 at 17:00. During this period the visibility was higher than 10 km and averaged hourly TSP was 187 ± 107 μg m^{-3}. The higher wind speeds (2.4 ± 0.6 m s^{-1}) during this period are more beneficial for atmospheric diffusion in comparison with the remaining periods. (2) Light-haze period, from December 5 at 18:00 to December 9 at 20:00. Visibility decreased to the range of 5–10 km in most hours of this period. Averaged TSP concentration increased up to 415 ± 205 μg m^{-3}, more than 2 times higher than that in the Clean period. (3) Severe-haze period, from December 10 at 10:00 to the sampling end. Air quality was extremely poor during this period; the average visibility declined to less than 3 km. However, the average TSP concentration (530 ± 180 μg m^{-3}) was only slightly higher than that in the Light-haze hours. Wind speeds (1.3 ± 0.5 m s^{-1} and 1.4 ± 0.8 m s^{-1} in Light- and Severe-haze periods, Table 1) during the Light- and Severe-haze periods were comparable, but the relative humidity was obviously higher in the Severe-haze period (53 ± 19% and 73 ± 14% in Light- and Severe-haze periods, Table 1).

3.2. Major chemical species

3.2.1. Dust-related components

As shown in Fig. 1c, TSP concentration presented a temporal variation pattern similar to that of elemental Fe during the Clean and Light-haze periods, suggesting that the concentrations of TSP are dominated by the dust-related species in the two relatively dry periods (Cao et al., 2008; Wu et al., 2011). Concentrations of Fe and Ca in the samples

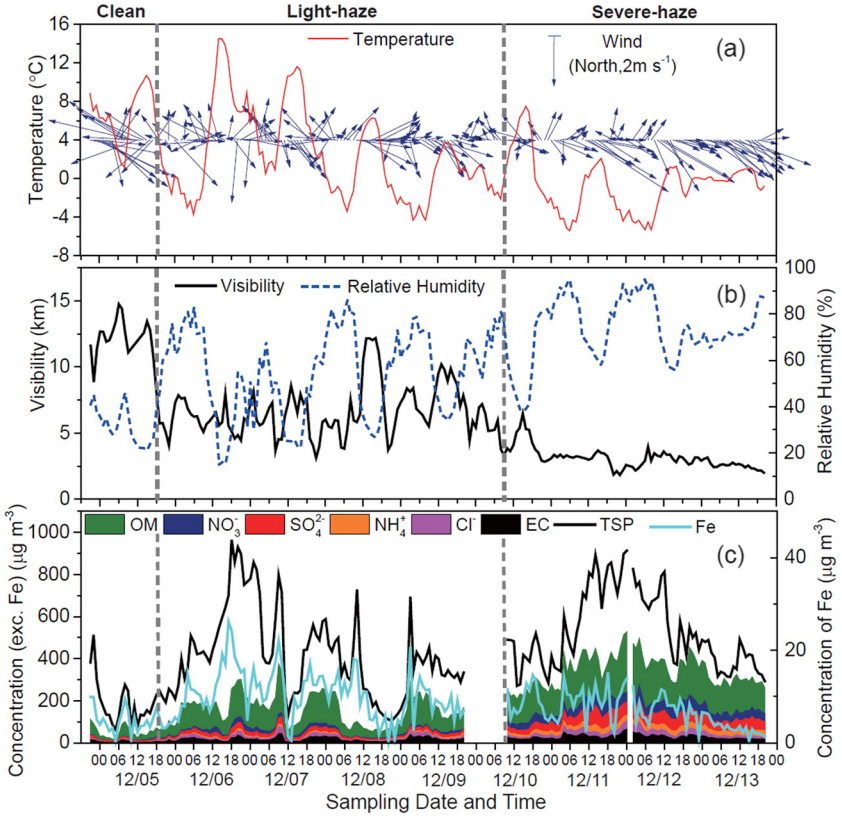

Fig. 1. Hourly variations in meteorological parameters and major chemical compositions of TSP during the sampling period in Xi'an (Clean period: 2012-12-4 21:00 to 2012-12-5 17:00; Light-haze period: 2012-12-5 18:00 to 2012.12.9 20:00; Severe-haze period: 2012-12-10 10:00 to 2012-12-13 20:00. OM means organic matter, calculated by OC*1.6).

Table 1
Meteorological conditions and concentrations of determined chemical compositions of TSP in the three sampling periods in Xi'an.

	Clean (N = 21)		Light-haze (N = 99)		Severe haze (N = 82)		S/L[a]
	Range	Ave. ± SD	Range	Ave. ± SD	Range	Ave. ± SD	
I. Meteorology parameters							
Wind speed (m s^{-1})	1.3–3.6	2.4 ± 0.6	0.0–2.5	1.3 ± 0.5	0.0–4.3	1.4 ± 0.8	
Temperature (°C)	1.2–10.7	6.7 ± 2.7	−4.3–14.5	2.7 ± 4.7	−5.4–7.5	−0.7 ± 2.9	
Relative humidity (%)	21–46	32 ± 8	15–86	53 ± 19	38–95	73 ± 14	
Visibility (km)	8.9–14.7	12.3 ± 1.3	3.1–12.2	6.8 ± 2.0	1.8–6.5	3.1 ± 0.8	
II. Major chemical species (μg m^{-3})							
TSP	63–514	187 ± 107	104–966	415 ± 205	271–913	530 ± 180	1.3
OC	4.2–44	19 ± 12	19–149	61 ± 29	72–180	108 ± 24	1.8
EC	1.8–16	6.2 ± 4.6	4.4–45	18 ± 9.4	17–65	29 ± 10	1.7
WSOC[b]	3.1–23	8.9 ± 4.9	6.3–141	26 ± 18	29–106	53 ± 14	2.1
WSIC[b]	2.4–6.2	4.2 ± 1.1	1.9–13	6.3 ± 1.8	0.1–8.1	3.6 ± 2	0.6
SO_4^{2-}	5.0–15	7.7 ± 2.6	6.8–35	16 ± 5.9	19–89	51 ± 15	3.3
NO_3^-	0.8–7	3 ± 1.7	2.9–31	12 ± 6.7	21–68	44 ± 9.7	3.6
NH_4^+	0.0–1.5	0.7 ± 0.4	0.3–13	4.1 ± 2.8	9.5–34	23 ± 5.6	5.6
Ca^{2+}	4.1–11	7.1 ± 1.8	1.3–21	9.9 ± 3.1	2.9–23	11 ± 4.3	1.1
K^+	0.3–1.5	0.6 ± 0.3	0.2–7.9	2.1 ± 1.4	1.7–8.1	5.4 ± 1.4	2.6
Ca	6.2–28	14 ± 5.7	8.1–65	28 ± 12	3.2–47	21 ± 9.9	0.7
Fe	0.3–9.9	4.8 ± 2.6	0.3–26	10 ± 5.2	0.5–15	7.1 ± 3.7	0.7
III. Primary organic markers (ng m^{-3})							
Hopanes	na[c]–7	3.0 ± 2.0	1.7–95	33 ± 24	1.5–161	38 ± 29	1.2
Dehydrated sugars[d]	17–236	94 ± 71	124–5814	1203 ± 1146	185–6835	2417 ± 1368	2.0
Other sugars[d]	4–84	31 ± 23	38–1381	210 ± 200	39–655	236 ± 123	1.1
PAHs	5–55	22 ± 12	29–649	193 ± 141	44–1459	350 ± 228	1.8
n-Alkanes	43–447	167 ± 90	153–2626	1118 ± 677	136–4706	1662 ± 834	1.5
Dehydroabietic acid	2.0–42	15 ± 10	25–798	197 ± 192	20–1136	289 ± 212	1.5
IV. Secondary organic markers (ng m^{-3})							
o-Phthalic acid	0.8–16	6.3 ± 4.5	10–142	51 ± 29	28–487	169 ± 86	3.3
Succinic acid	1.8–18	7.1 ± 4.4	6.1–52	22 ± 11	16–115	49 ± 25	2.2
2,3-Dihydroxy-4-oxopentanoic acid	0.8–5.5	1.9 ± 1.1	2.7–23	9.2 ± 4.6	na–35	17 ± 7.9	1.9

[a] S/L: ratio of the concentration in Severe-haze period (S) to Light-haze period (L).
[b] WSOC: water soluble organic carbon; WSIC: water soluble inorganic carbon; WSON: water soluble organic nitrogen.
[c] na: not available.
[d] Dehydrated sugars: sum of galactosan, mannosan, and levoglucosan; other sugars: sum of arabitol, fructose, glucose, mannitol, inositol, sucrose, and trehalose.

collected during the Severe-haze period decreased obviously, being 0.7 times of those in the Light-haze period (Table 1). Water soluble Ca^{2+} presented comparable concentrations in the two haze periods (9.9 ± 3.1 μg m^{-3} in the Light-haze and 11 ± 4.3 μg m^{-3} in the Severe-haze periods, respectively). In contrast, other water-soluble ions increased at least two times in the Severe-haze period. Robust linear correlation between Fe and TSP was only found in the Clean and Light-haze periods (R^2 = 0.72, Fig. 2a), indicating an important contribution of dust-related

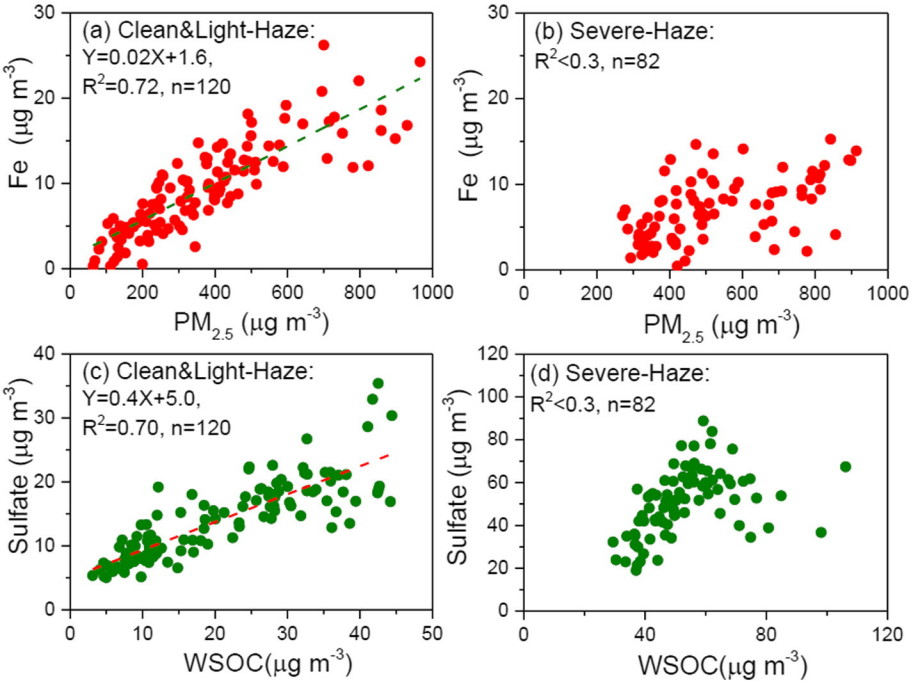

Fig. 2. Linear fit regressions for TSP with Fe (a and b) and WSOC with sulfate (c and d) in the lower RH (Clean and Light-haze) periods and higher RH (Severe-haze) period.

emissions to TSP in these two periods rather than in the Severe-haze period (R^2<0.3, Fig. 2b).

As shown in Table 1 and Fig. S2, the city is controlled by the high pressure, and the temperature and wind speed were very low during the Light-haze period. Under such a stagnant condition, aerosols in the atmosphere of Xi'an should be mostly derived from the local sources rather than from long-range transport. Thus, it is plausible that the high contribution of dust-related species to TSP concentration during the Light-haze period is mainly derived from the local construction activities, bare soils and unpaved road dust (Han et al., 2007).

3.2.2. Secondary inorganic ions

As shown in Fig. 1c and Table 1, concentrations of SO_4^{2-}, NO_3^-, and NH_4^+ (SNA) increased dramatically during the Severe-haze period, being 3.3 − 5.6 times of those in the Light-haze period. Such increases in secondary inorganic ions during a hazy period have been found in many other Chinese urban regions including Beijing (Y. Sun et al., 2013, 2014), Tianjing (Han et al., 2014), Shanghai (Wang et al., 2014a), and Guangzhou (Tan et al., 2009), of which the meteorological condition is characteristic of low visibility and high relative humidity. During such a hazy period solar radiation is weak and O_3 level is low, which suggests that photochemical oxidation is inactive. Thus, the above enhanced production of the secondary SNA during the Severe-haze period should be attributable to effective aerosol aqueous-phase oxidation (Y. Sun et al., 2013; Wang et al., 2014b), specifically, the aqueous phase formation of sulfate. Relative humidity during the Severe-haze period was higher (73 ± 14%, Table 1) and temperature was lower (−0.7 ± 2.9 °C). Such meteorological conditions are favorable for the heterogeneous uptake of gaseous SO_2 on deliquesced aerosols and subsequent oxidation of the S (IV) into sulfate (Wang et al., 2014b). On the other hand, ammonia is also abundant in Guanzhong basin (unpublished data), which could react with sulfate and neutralize the aerosol aqueous phase, further promoting the formation of sulfate.

3.2.3. Carbonaceous fractions

A few field measurements have suggested that organic components, especially for secondary organic aerosols (SOAs), play an important role in haze formation process (Guo et al., 2014; Huang et al., 2014). SOA in the atmosphere is produced from photo-oxidation of various anthropogenic and biogenic VOCs (volatile organic compounds) (Hallquist et al., 2009) and abundant in hydrophilic carboxylic, hydroxyl and/or carbonyl species (Aggarwal et al., 2013; Wang et al., 2012), which are water soluble species. In the present study, the concentration of OC in the Severe-haze period was 1.8 times of that in the Light-haze period and 5.7 times of those in the Clean period. As shown in Table 1, concentration of water-soluble organic carbon (WSOC), which is mainly consisted of organics containing carboxylic, carbonyl and hydroxyl groups, in the Severe-haze period was 2.1 times of that in the Light-haze period, suggesting an enhanced formation of SOA in the humid period. However, the increasing extent of WSOC (2.1 times) was lower than that of secondary inorganic aerosols (3.3 − 5.6 times), probably suggesting that SOA production is less efficient compared to sulfate and nitrate.

In contrast to WSOC, atmospheric WSIC (water-soluble inorganic carbon) consisted of CO_3^{2-} and/or HCO_3^- and derived mainly from dust-related sources (Ho et al., 2012). Their concentrations (Table 1) in the two haze periods were comparable, although other carbon fractions increased obviously during the latter haze event.

3.2.4. Mass closure of TSP

The relative contributions of major chemical species to the TSP concentration in the three periods are shown in Fig. 3. The most important fraction in the whole sampling period is organic matter (OM, calculated by OC*1.6) (Turpin et al., 2000), being consistent with those reported by other studies (Huang et al., 2014). The relative contributions of OM to TSP in the Light- and Severe-haze periods are 1.4 and 2.0 times of that in the Clean period, respectively, indicating an important role of organic

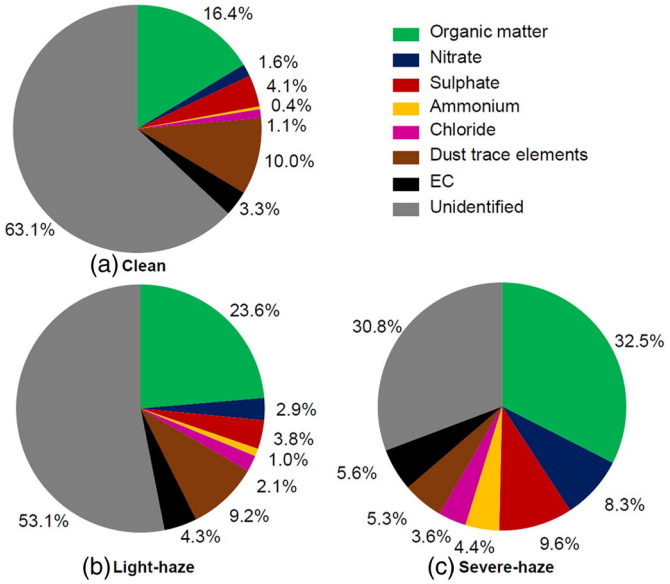

Fig. 3. Chemical compositions of TSP in the Clean, Light-, and Severe-haze periods. Organic matter is calculated by OC*1.6.

aerosols in haze formation process in Xi'an. The relative contribution of secondary inorganic ions (i.e., SO_4^{2-}, NO_3^- and NH_4^+) to the TSP mass enhanced slightly in the Light-haze period (7.7%) compared to that in the Clean period (6.1%), but it increased dramatically in the Severe-haze period (22.3%). Such a result is consistent with that reported by Huang et al. (2014), and further demonstrates that secondary inorganic aerosols also have an important role in haze formation process. As described above, the emission of dust-related sources decreased in the Severe-haze period, thus the relative contributions (5.3%) of dust trace elements (sum of Fe and Ca) and unidentified fractions (31%) to TSP were lower than that in the Clean (10% and 63%) and Light-haze (9.2% and 53%) periods.

3.3. Organic compounds

3.3.1. Primary organic markers

In the current study, about fifty organic compounds were determined to qualitatively analyze the relative contribution of anthropogenic emissions from coal combustion, vehicle exhaust and biomass burning (Table 1 and S1). 17α(H), 21β(H)-30-norhopane($C_{29\alpha\beta}$) and 17α(H),21β(H)-hopane($C_{30\alpha\beta}$) are mainly emitted from coal burning and internal combustion engines (Kawamura et al., 1995; Simoneit et al., 2004c). Their concentrations in the Light-haze period were about one order of magnitude higher than those in the Clean period, but comparable with those in the Severe-haze period. It is plausible that the emission strengths of coal burning and vehicle exhaust were relatively stable in the urban area within the sampling days; the increases in hopane concentrations in the two haze episodes were mainly caused by accumulation effect due to the stagnant conditions. Concentrations of the dehydrated sugars (i.e., galactosan, mannosan and levoglucosan) increased by an order of magnitude in the Light-haze period compared to that in the Clean period and further increased during the Severe-haze hours, suggesting an enhanced emission of biomass burning (Engling et al., 2009; Simoneit et al., 2004a) in the Severe-haze time. Both hopanes and levoglucosan presented a similar day and night variation pattern with the highest at midnight (Fig. 4), but the ratio of levoglucosan to 17α(H), 21β(H)-30-norhopane presented higher values at nighttime, which can be ascribed to the enhanced biomass burning emission due to house heating in the rural areas around the city. Dehydroabietic acid is also a typical tracer for biomass burning smoke (Simoneit,

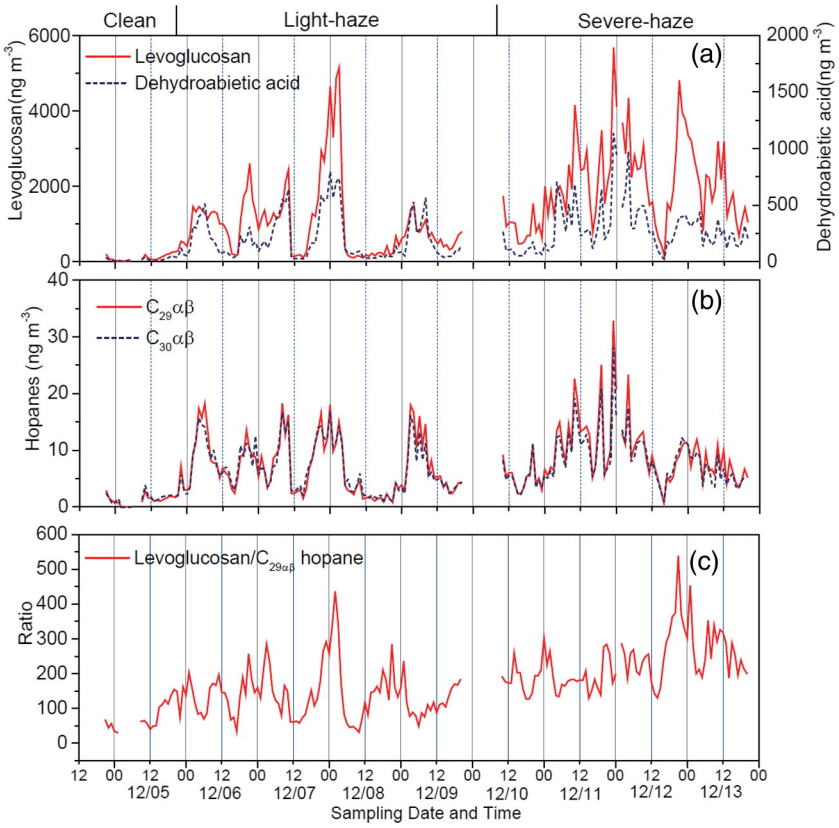

Fig. 4. Hourly variations in concentrations of hopanes, levoglucosan, and dehydroabietic acid in the TSP samples during the whole sampling period in Xi'an.

2002). Thus it presented a strong correlation with levoglucosan (R^2 = 0.72) (Table 1 and Fig. 4a).

Due to accumulation effect under the stagnant meteorological condition, concentrations of *n*-alkanes and polycyclic aromatic hydrocarbons (PAHs) in the two haze periods are significantly higher than those in the Clean period. Their higher concentrations (1662 ± 834 and 350 ± 228 ng m^{-3}) in the Severe-haze period compared to those (1118 ± 677 and 193 ± 141 ng m^{-3}) in the Light-haze period also resulted in part from the enhanced biomass burning emission in the rural areas. Fig. 5 shows the hourly change of diagnostic ratios of *n*-alkanes and PAHs. *n*-Alkanes derived from fossil fuel combustion do not have odd/even carbon number preference. However, *n*-alkanes derived from terrestrial plant emissions are dominated by high molecular weight species (HMW, carbon number >25) and characterized by an odd number of carbon preference index (CPI) larger than 5 (Rogge et al., 1993; Simoneit et al., 2004b, 2004c). As shown in Fig. 5a, CPI of total *n*-alkanes (C_{18}–C_{36}) in the whole sampling period was 1.3 ± 0.1 (0.8–1.5) with no significant differences among the Clean, Light-haze and Severe-haze periods, indicating that *n*-alkanes during the sampling period were mostly derived from fossil fuel combustion. However, CPI of HMW *n*-alkanes presented higher values at nighttime than daytime, which can be explained by the enhanced biomass burning activities due to house heating, because HMW *n*-alkanes that are of larger CPI values can be directly emitted from incomplete combustion of biomass such as wheat straw (Wang et al., 2009).

Previous studies reported that diagnostic ratios of Flu/(Flu + Pyr) in the smokes from gasoline, diesel, and coal combustions are >0.50, <0.50, and ~0.58 (Agudelo-Castañeda and Teixeira, 2014; Ravindra et al., 2006, 2008; Teixeira et al., 2013), and the ratios of IP/BghiP from the above smokes are 0.2, 0.5, and 1.3 (Ohura et al., 2004), respectively. In addition, BghiP/BeP are 2.0 and 0.8 in emissions from vehicle exhaust and coal burning smoke (Grimmer et al., 1981). In the current study, ratios of Flu/(Flu + Pyr) in the TSP samples were 0.56 ± 0.04 (Fig. 5b), which is close to the ratio of aerosols from coal combustion. IP/BghiP and BghiP/BeP in the current study were 1.0 ± 0.1 and 0.8 ± 0.2 (Fig. 5c and d), respectively, which are also closer to the values for coal combustion, suggesting that PAHs in the city are mostly emitted by residential coal burning for house heating and cooking. As seen in Fig. 5b-d, the diagnostic ratios varied slightly, further indicating that the coal burning is the dominant source of PAHs. However, the ratio of BaP/BeP showed a significant day-night variation with lower value (0.78 ± 0.18) in daytime than that (0.92 ± 0.19) in nighttime (Fig. 5e). BaP is labile to photochemical degradation while its isomer BeP is much stable (Ohkouchi et al., 1999; Okuda et al., 2002), thus the lower value of BaP/BeP can be explained by the stronger daytime photochemical degradation. The average ratios of BaP/BeP were 0.70, 0.86 and 0.87 in the Clean, Light-haze and Severe-haze periods, respectively, while the day/night ratios of BaP/BeP were 0.79 during the Light-haze period and 0.94 during the Severe-haze period. Such enhanced ratios in the heavy haze hours should be caused by a decreased photochemical oxidation under the low visibility condition.

3.3.2. Secondary organic markers

In the current study, *o*-phthalic acid, succinic acid, and 2,3-dihydroxy-4-oxopentanoic acid are determined and can be roughly considered as indicators for secondary organic aerosols. *o*-Phthalic acid is believed to be produced by the oxidation of naphthalene and other PAHs (Kawamura and Ikushima, 1993; Kawamura et al., 2005). 2,3-Dihydroxy-4-oxopentanoic acid is a compound derived from toluene oxidation (Kleindienst et al., 2004, 2007), while succinic acid can be formed from photochemical oxidation of unsaturated hydrocarbons and fatty acids emitted from biomass burning and coal combustion (Kawamura and Yasui, 2005; Wang et al., 2010). A few studies have proved that the above precursors, which are volatile or semi-volatile organic compounds, are highly abundant in the atmosphere of urban regions of China (P.Q. Fu et al., 2008; Guo et al., 2014; Ma et al., 2011). In the

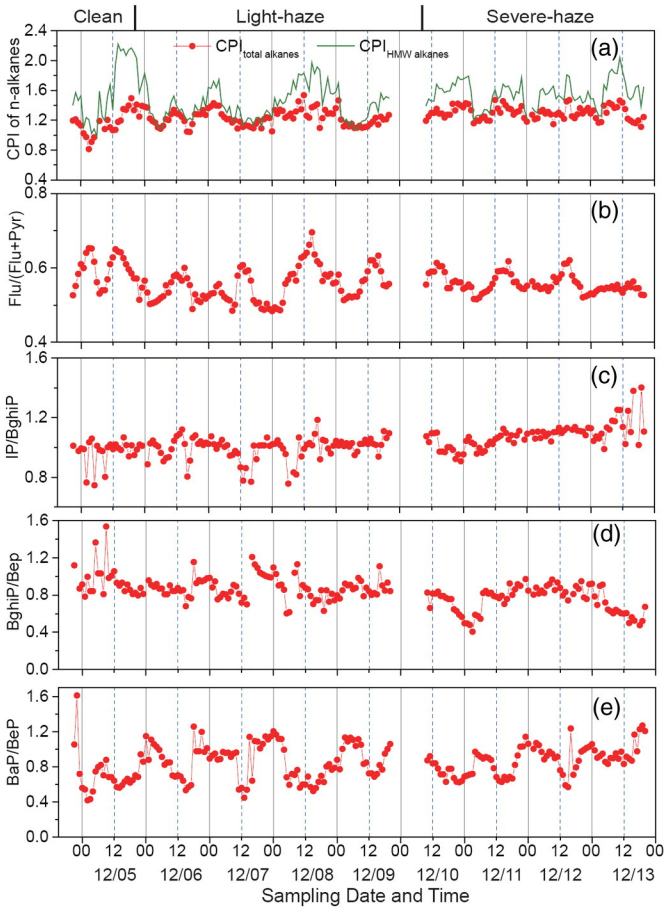

Fig. 5. Hourly variations in diagnostic ratios of *n*-alkanes and PAHs in TSP during the whole sampling period in Xi'an.

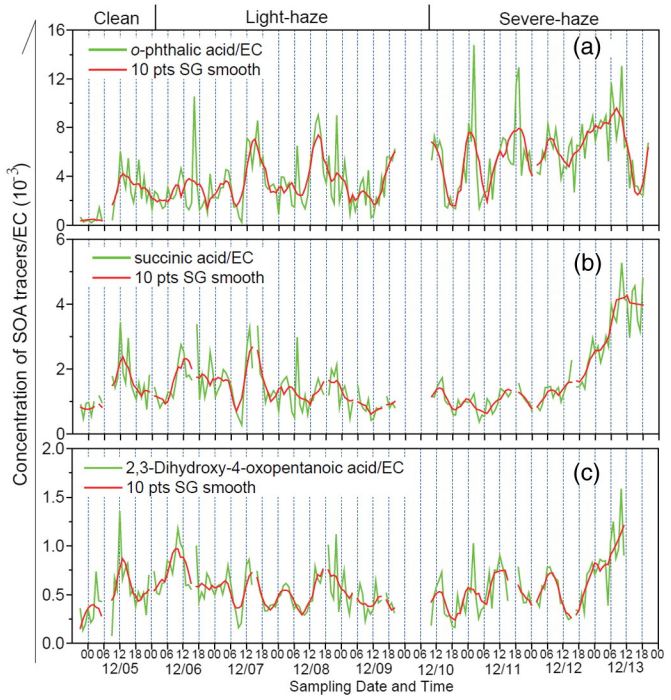

Fig. 6. Hourly variations in the ratios of three secondary organic aerosol tracers/EC in TSP during the whole sampling period in Xi'an.

current study, averaged concentrations of the three secondary organic markers in the Severe-haze period were 1.9–3.3 times of those in the Light-haze period. Such differences are more significant than that of the POA indicators discussed above. As shown in Fig. 6, these secondary compounds presented a continuously increasing trend, indicating an enhanced production of secondary organic aerosols during the Severe-haze period, which is probably caused by the enhanced partitioning of secondary water-soluble organic gases into the aerosol aqueous phase under the high RH condition. As seen in Fig. S3, *o*-phthalic acid showed a good correlation ($R^2 = 0.43$) with liquid water content (LWC) of particles in the atmosphere. LWC of particles in the Severe-haze period was much higher (178 ± 190 μg m^{-3}), and *o*-phthalic acid is a moderate water-soluble compound (water-solubility = 0.6 g/100 mL at 25 °C) (http://hazard.com/msds/mf/baker/baker/files/p4270.htm). Thus, the increased concentration of *o*-phthalic in the Severe-haze hours can be partly explained by the enhanced gas-to-aerosol aqueous phase partitioning. However, more chamber and field studies are warranted in order to understand the exact influence of high RH condition on SOA and haze formation in China.

4. Conclusion

Two types of haze episodes, Light-haze and Severe-haze, in Xi'an during the winter of 2012 were identified based on the differences in visibility and relative humidity. The Light-haze period is characteristic of low RH ($53 \pm 19\%$) and moderate impairment (6.8 ± 2.0 km) in visibility while the Severe-haze period is characterized by high RH ($73 \pm 14\%$) and extremely low visibility (3.1 ± 0.8 km), although TSP presented a similar level in both events. Chemical compositions and sources of TSP within the two types of haze hours were significantly different. Elemental Fe and Ca (28 ± 12 and 10 ± 5.2 μg m^{-3}) in the Light-haze period presented much higher concentrations and well correlated with TSP concentrations, suggesting that the Light-haze period is attributed to dust suspension. SO_4^{2-}, NO_3^- and NH_4^+ within the Severe-haze period increased dramatically to 51 ± 15, 44 ± 9.7 and 23 ± 5.6 μg m^{-3}, accounting for 9.6%, 8.3% and 4.4% of the TSP mass, respectively, indicating that secondary oxidation-derived particles are responsible for the haze formation.

Compared to those in the Clean period primary organic aerosols such as hopanes, *n*-alkanes, PAHs and dehydrated sugars of TSP are about ten times higher in the Light-haze period and twenty times higher in the Severe-haze period, which is mainly due to the accumulation effect under the wintertime stagnant conditions. *n*-Alkanes and PAHs in the Light-haze period showed similar compositions to those in the Severe-haze period and are characterized by fossil fuel combustion emissions. Enhanced BaP/BeP ratios in the heavy haze hours should be caused by a decreased photochemical oxidation. Compared to those in the Light-haze period relative abundances of *o*-phthalic and succinic acids to EC increased by a factor of 1.1–1.7, probably indicating that the humid conditions in the Severe-haze periods were favorable for the partitioning of gas-phase water-soluble organics into the aerosol phase, resulting in a higher production of SOA.

Acknowledgements

This work was financially supported by the China National Natural Science Founds for Distinguished Young Scholars (no. 41325014), the Strategic Priority Research Program of the Chinese Academy of Sciences (grants 41325014, XDA05100103, and XDB05020401) and the program from National Natural Science Foundation of China (no. 41405122).

Appendix A. Supplementary data

Supplementary data to this article can be found online at http://dx.doi.org/10.1016/j.scitotenv.2016.05.057.

References

Aggarwal, S.G., Kawamura, K., Umarji, G.S., Tachibana, E., Patil, R.S., Gupta, P.K., 2013. Organic and inorganic markers and stable C-, N-isotopic compositions of tropical coastal aerosols from megacity Mumbai: sources of organic aerosols and atmospheric processing. Atmos. Chem. Phys. 13, 4667–4680.

Agudelo-Castañeda, D.M., Teixeira, E.C., 2014. Seasonal changes, identification and source apportionment of PAH in PM1.0. Atmos. Environ. 96, 186–200.

Cao, J.J., Chow, J.C., Watson, J.G., Wu, F., Han, Y.M., Jin, Z.D., et al., 2008. Size-differentiated source profiles for fugitive dust in the Chinese Loess Plateau. Atmos. Environ. 42, 2261–2275.

Engling, G., Lee, J.J., Tsai, Y.W., Lung, S.C.C., Chou, C.C.K., Chan, C.Y., 2009. Size-resolved anhydrosugar composition in smoke aerosol from controlled field burning of rice straw. Aerosol Sci. Technol. 43, 662–672.

Fu, P.Q., Kawamura, K., Okuzawa, K., Aggarwal, S.G., Wang, G.H., Kanaya, Y., et al., 2008. Organic molecular compositions and temporal variations of summertime mountain aerosols over Mt. Tai, North China Plain. J. Geophys. Res.-Atmos. 113, D19107. http://dx.doi.org/10.1029/2008JD009900.

Fu, Q., Zhuang, G., Wang, J., Xu, C., Huang, K., Li, J., et al., 2008. Mechanism of formation of the heaviest pollution episode ever recorded in the Yangtze River Delta, China. Atmos. Environ. 42, 2023–2036.

Grimmer, G., Jacob, J., Naujack, K.W., Dettbarn, G., 1981. Profile of the polycyclic aromatic hydrocarbons from used engine oil—inventory by GCGC/MS—PAH in environmental materials, part 2. Fresenius' Z. Anal. Chem. 309, 13–19.

Guo, S., Hu, M., Zamora, M.L., Peng, J., Shang, D., Zheng, J., et al., 2014. Elucidating severe urban haze formation in China. Proc. Natl. Acad. Sci. U. S. A. 111, 17373–17378.

Hallquist, M., Wenger, J.C., Baltensperger, U., Rudich, Y., Simpson, D., Claeys, M., et al., 2009. The formation, properties and impact of secondary organic aerosol: current and emerging issues. Atmos. Chem. Phys. 9, 5155–5236.

Han, L., Zhuang, G., Cheng, S., Wang, Y., Li, J., 2007. Characteristics of re-suspended road dust and its impact on the atmospheric environment in Beijing. Atmos. Environ. 41, 7485–7499.

Han, S.Q., Wu, J.H., Zhang, Y.F., Cai, Z.Y., Feng, Y.C., Yao, Q., et al., 2014. Characteristics and formation mechanism of a winter haze-fog episode in Tianjin, China. Atmos. Environ. 98, 323–330.

Ho, S.S.H., Ho, K.F., Liu, S.X., Liu, W.D., Lee, S.C., Fung, K.K., et al., 2012. Quantification of carbonate carbon in aerosol filter samples using a modified thermal/optical carbon analyzer (M-TOCA). Anal. Methods 4, 2578–2584.

Huang, R.-J., Zhang, Y., Bozzetti, C., Ho, K.-F., Cao, J.-J., Han, Y., et al., 2014. High secondary aerosol contribution to particulate pollution during haze events in China. Nature 514, 218–222.

Kawamura, K., Ikushima, K., 1993. Seasonal changes in the distribution of dicarboxylic acids in the urban atmosphere. Environ. Sci. Technol. 27, 2227–2235.

Kawamura, K., Yasui, O., 2005. Diurnal changes in the distribution of dicarboxylic acids, ketocarboxylic acids and dicarbonyls in the urban Tokyo atmosphere. Atmos. Environ. 39, 1945–1960.

Kawamura, K., Kosaka, M., Sempere, R., 1995. Distributions and seasonal changes in hydrocarbons in urban aerosols and rain waters. Chikyu Kagaku (Geochemistry) 29, 1–15 (In Japanese).

Kawamura, K., Imai, Y., Barrie, L.A., 2005. Photochemical production and loss of organic acids in high Arctic aerosols during long-range transport and polar sunrise ozone depletion events. Atmos. Environ. 39, 599–614.

Kleindienst, T.E., Conver, T.S., McIver, C.D., Edney, E.O., 2004. Determination of secondary organic aerosol products from the photooxidation of toluene and their implications in ambient PM2.5. J. Atmos. Chem. 47, 79–100.

Kleindienst, T.E., Jaoui, M., Lewandowski, M., Offenberg, J.H., Lewis, C.W., Bhave, P.V., et al., 2007. Estimates of the contributions of biogenic and anthropogenic hydrocarbons to secondary organic aerosol at a southeastern US location. Atmos. Environ. 41, 8288–8300.

Li, J., Wang, G., Aggarwal, S.G., Huang, Y., Ren, Y., Zhou, B., et al., 2014. Comparison of abundances, compositions and sources of elements, inorganic ions and organic compounds in atmospheric aerosols from Xi'an and New Delhi, two megacities in China and India. Sci. Total Environ. 476–477, 485–495.

Ma, W.L., Sun, D.Z., Shen, W.G., Yang, M., Qi, H., Liu, L.Y., et al., 2011. Atmospheric concentrations, sources and gas-particle partitioning of PAHs in Beijing after the 29th Olympic Games. Environ. Pollut. 159, 1794–1801.

Menon, S., Hansen, J., Nazarenko, L., Luo, Y.F., 2002. Climate effects of black carbon aerosols in China and India. Science 297, 2250–2253.

Ohkouchi, N., Kawamura, K., Kawahata, H., 1999. Distributions of three- to seven-ring polynuclear aromatic hydrocarbons on the deep sea floor in the central Pacific. Environ. Sci. Technol. 33, 3086–3090.

Ohura, T., Amagai, T., Fusaya, M., Matsushita, H., 2004. Polycyclic aromatic hydrocarbons in indoor and outdoor environments and factors affecting their concentrations. Environ. Sci. Technol. 38, 77–83.

Okuda, T., Kumata, H., Zakaria, M.P., Naraoka, H., Ishiwatari, R., Takada, H., 2002. Source identification of Malaysian atmospheric polycyclic aromatic hydrocarbons nearby forest fires using molecular and isotopic compositions. Atmos. Environ. 36, 611–618.

Quan, J., Zhang, Q., He, H., Liu, J., Huang, M., Jin, H., 2011. Analysis of the formation of fog and haze in North China Plain (NCP). Atmos. Chem. Phys. 11, 8205–8214.

Ravindra, K., Bencs, L., Wauters, E., de Hoog, J., Deutsch, F., Roekens, E., et al., 2006. Seasonal and site-specific variation in vapour and aerosol phase PAHs over Flanders (Belgium) and their relation with anthropogenic activities. Atmos. Environ. 40, 771–785.

Ravindra, K., Sokhi, R., Vangrieken, R., 2008. Atmospheric polycyclic aromatic hydrocarbons: source attribution, emission factors and regulation. Atmos. Environ. 42, 2895–2921.

Rogge, W.F., Hildemann, L.M., Mazurek, M.A., Cass, G.R., Simoneit, B.R.T., 1993. Sources of fine organic aerosols. 4. Particulate abrasion products from leaf surfaces of urban plants. Environ. Sci. Technol. 27, 2700–2711.

Simoneit, B.R.T., 2002. Biomass burning - a review of organic tracers for smoke from incomplete combustion. Appl. Geochem. 17, 129–162.

Simoneit, B.R.T., Elias, V.O., Kobayashi, M., Kawamura, K., Rushdi, A.I., Medeiros, P.M., et al., 2004a. Sugars - dominant water-soluble organic compounds in soils and characterization as tracers in atmospheric particulate matter. Environ. Sci. Technol. 38, 5939–5949.

Simoneit, B.R.T., Kobayashi, M., Mochida, M., Kawamura, K., Huebert, B.J., 2004b. Aerosol particles collected on aircraft flights over the northwestern Pacific region during the ACE-Asia campaign: composition and major sources of the organic compounds. J. Geophys. Res.-Atmos. 109, D19S09. http://dx.doi.org/10.1029/2004JD004565.

Simoneit, B.R.T., Kobayashi, M., Mochida, M., Kawamura, K., Lee, M., Lim, H.J., et al., 2004c. Composition and major sources of organic compounds of aerosol particulate matter sampled during the ACE-Asia campaign. J. Geophys. Res.-Atmos. 109, D19S10. http://dx.doi.org/10.1029/2004JD004598.

Streets, D.G., Waldhoff, S.T., 2000. Present and future emissions of air pollutants in China: SO_2, NOx, and CO. Atmos. Environ. 34, 363–374.

Sun, Y., Wang, Z., Fu, P., Jiang, Q., Yang, T., Li, J., et al., 2013. The impact of relative humidity on aerosol composition and evolution processes during wintertime in Beijing, China. Atmos. Environ. 77, 927–934.

Sun, Y.L., Wang, Z.F., Fu, P.Q., Yang, T., Jiang, Q., Dong, H.B., et al., 2013. Aerosol composition, sources and processes during wintertime in Beijing, China. Atmos. Chem. Phys. 13, 4577–4592.

Sun, Y., Jiang, Q., Wang, Z., Fu, P., Li, J., Yang, T., et al., 2014. Investigation of the sources and evolution processes of severe haze pollution in Beijing in January 2013. J. Geophys. Res. Atmos. 119 (2014JD021641).

Tan, J.-H., Duan, J.-C., Chen, D.-H., Wang, X.-H., Guo, S.-J., Bi, X.-H., et al., 2009. Chemical characteristics of haze during summer and winter in Guangzhou. Atmos. Res. 94, 238–245.

Teixeira, E.C., Mattiuzi, C.D., Agudelo-Castaneda, D.M., Garcia Kde, O., Wiegand, F., 2013. Polycyclic aromatic hydrocarbons study in atmospheric fine and coarse particles using diagnostic ratios and receptor model in urban/industrial region. Environ. Monit. Assess. 185, 9587–9602.

Turpin, B.J., Saxena, P., Andrews, E., 2000. Measuring and simulating particulate organics in the atmosphere: problems and prospects. Atmos. Environ. 34, 2983–3013.

van Donkelaar, A., Martin, R.V., Brauer, M., Kahn, R., Levy, R., Verduzco, C., et al., 2010. Global estimates of ambient fine particulate matter concentrations from satellite-based aerosol optical depth: development and application. Environ. Health Perspect. 118, 847–855.

Wang, G.H., Kawamura, K., Xie, M.J., Hu, S.Y., Cao, J.J., An, Z.S., et al., 2009. Organic molecular compositions and size distributions of chinese summer and autumn aerosols from Nanjing: characteristic haze event caused by wheat straw burning. Environ. Sci. Technol. 43, 6493–6499.

Wang, G., Xie, M., Hu, S., Gao, S., Tachibana, E., Kawamura, K., 2010. Dicarboxylic acids, metals and isotopic compositions of C and N in atmospheric aerosols from inland China: implications for dust and coal burning emission and secondary aerosol formation. Atmos. Chem. Phys. 10, 6087–6096.

Wang, G.H., Kawamura, K., Cheng, C.L., Li, J.J., Cao, J.J., Zhang, R.J., et al., 2012. Molecular distribution and stable carbon isotopic composition of dicarboxylic acids, ketocarboxylic acids, and alpha-dicarbonyls in size-resolved atmospheric particles from Xi'an City, China. Environ. Sci. Technol. 46, 4783–4791.

Wang, Y., Li, L., Chen, C., Huang, C., Huang, H., Feng, J., et al., 2014a. Source apportionment of fine particulate matter during autumn haze episodes in Shanghai, China. J. Geophys. Res. Atmos. 119, 1903–1914.

Wang, Y., Zhang, Q., Jiang, J., Zhou, W., Wang, B., He, K., et al., 2014b. Enhanced sulfate formation during China's severe winter haze episode in January 2013 missing from current models. J. Geophys. Res. Atmos. 119, 10425–10440.

Wu, F., Chow, J.C., An, Z., Watson, J.G., Cao, J., 2011. Size-differentiated chemical characteristics of Asian paleo dust: records from Aeolian deposition on Chinese Loess Plateau. J. Air Waste Manage. Assoc. 61, 180–189.

Xi'an Municipal Bureau of Statistics, NBS Survey Office in Xi'an, 2013i. Xi'an Statistical Yearbook. China Statistics Press, Beijing.

Ye, X., Ma, Z., Zhang, J., Du, H., Chen, J., Chen, H., et al., 2011. Important role of ammonia on haze formation in Shanghai. Environ. Res. Lett. 6, 024019.

Zhang, Q., Shen, Z., Cao, J., Zhang, R., Zhang, L., Huang, R.J., et al., 2015. Variations in PM2.5, TSP, BC, and trace gases (NO_2, SO_2, and O_3) between haze and non-haze episodes in winter over Xi'an, China. Atmos. Environ. 112, 64–71.

Zhao, X.J., Zhao, P.S., Xu, J., Meng, W., Pu, W.W., Dong, F., et al., 2013. Analysis of a winter regional haze event and its formation mechanism in the North China Plain. Atmos. Chem. Phys. 13, 5685–5696.

Zhao, M., Qiao, T., Huang, Z., Zhu, M., Xu, W., Xiu, G., et al., 2015. Comparison of ionic and carbonaceous compositions of PM2.5 in 2009 and 2012 in Shanghai, China. Sci. Total Environ. 536, 695–703.